TUNABLE ALL OPTICAL SWITCH IMPLEMENTED IN A LIQUID CRYSTAL FILLED DUAL-CORE PHOTONIC CRYSTAL FIBER

K. R. Khan[1, *], S. Bidnyk[1, 2], and T. J. Hall[1]

[1]School of Electrical Engineering and Computer Science, University of Ottawa, 800 King Edward Avenue, Ottawa, ON K1N6N5, Canada

[2]Enablence Technologies Inc., 400 March Road, Ottawa, ON K2K3H4, Canada

Abstract—We propose an all optical switch in a dual-core photonic crystal fiber (PCF) that has the core region consisting of soft glass and has nematic liquid crystal filled holes in the cladding region. Light waves are guided in this PCF by total internal reflection (TIR) due to the refractive index contrast between soft glass and liquid crystal (LC). Its wavelength dependent coupling, birefringence and dispersion are calculated and later use these parameters to evaluate the switching characteristics of short pulses propagating through this optical waveguide. The switch demonstrates tunability with external perturbation such as applying external heat source or electric field. Refractive index sensitivity of LC with these perturbation as well as polarization of the light signal determines the coupling, birefringence and dispersion properties of the overall waveguide and its switching characteristics.

1. INTRODUCTION

Researchers explored new physical properties of PCFs by filling air cylinders in the cladding region with isotropic or anisotropic materials instead of air [1–4]. Other types of doped and undoped PCFs were also studied [5, 6]. Most recently, liquid crystal filled photonic crystal fiber (LC-PCF) has attracted a considerable amount of attention [7, 8] due to its unique wave guiding properties. In particular, the presence of liquid crystal has been demonstrated to make fiber sensitive to external perturbation, such as change of temperature, pressure, external electric

field, rubbing angle etc. [8–10]. In this paper, we propose an all optical switch implemented in a PCF comprising a central core region of soft glass (SF57) surrounded by holes infiltrated with E7 type nematic liquid crystal. Waves are guided in this PCF by total internal reflection (TIR) due to the refractive index difference between soft glass and LC. Modal characteristics of regular dual core PCFs with air filled cladding holes were investigated by using the vector finite element method (FEM) [11–13]. In this study, we used the similar numerical tools to evaluate wavelength dependent dispersion and coupling characteristics of LC-PCF couplers. The results were found to be in good agreement with the ones obtained using other commercially available software (Fimwave from Photon Design Inc.) [14]. Using the finite difference method modal characteristics (confinement loss, dispersion and birefringence) of single core LC filled PCF are discussed in reference [15]. The same group also reported the coupling and polarization characteristics of the similar PCF with dual core [16–18]. Coupling and birefringence results obtained from our vector finite element based model qualitatively agree with their reported results. In this study, we primarily focus on PCF properties induced by the presence of anisotropic material (liquid crystal) and use our findings to assess the feasibility of building an all optical switch. We also demonstrate that the switch is tunable by applying external perturbation such as temperature change due to heating or applying external electric field.

2. GUIDED MODES IN DUAL CORE LC-PCF

Figure 1(a) shows the schematic of a dual core PCF, where the holes with diameter d and pitch Λ placed in the cladding region are infiltrated with E7 type nematic LC instead of air. Vector finite element method (FEM) was used to analyze the LC-PCF modes [12–14, 19]. The vector wave equation for the $\mathbf{E}$ field is given by,

$$\nabla \times \left(\frac{1}{\mu_r} \nabla \times \mathbf{E} \right) - k_0^2 n^2 \mathbf{E} = 0 \qquad (1)$$

where μ_r and n are the permeability and refractive index of the material in the waveguide respectively, k_0 is the free space wave number. The refractive index of both E7-LC and soft glass (SF57) are wavelength dependent [15, 20–24]. The soft glass of type SF57's refractive index can be evaluated by taking the square root of the permittivity expressed by the Sellmeier equation [15, 20–24]

$$\varepsilon_r(\lambda) = 1 + \sum_{n=1}^{3} \frac{B_n \lambda^2}{\lambda^2 - C_n} \qquad (2)$$
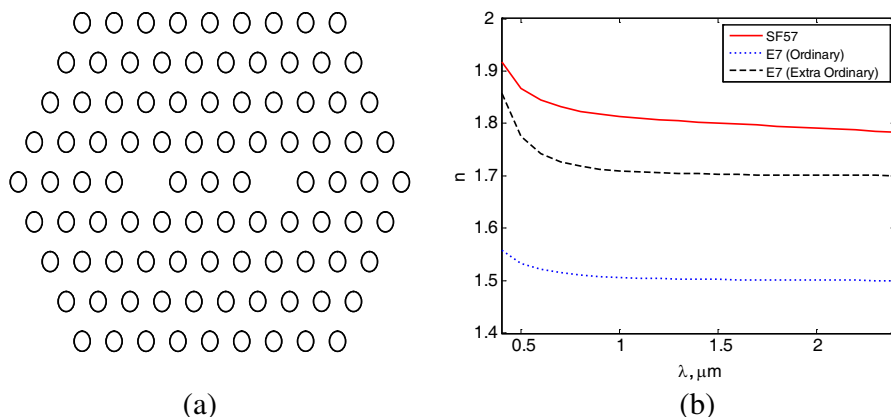
Figure 1. (a) Schematic diagram of dual core PCF with $d = 1\,\mu m$ and $d/\Lambda = 0.4$. (b) Refractive index of SF57 and E7, LC (both ordinary and extra ordinary) at $25°C$.

where coefficient $B_1 = 1.87543831$, $B_2 = 0.37375749$, $B_3 = 2.300001797$ and $C_1 = 0.0141749518$, $C_2 = 0.0640509927$, $C_3 = 177.389795$.

The other material E7's refractive indices are mainly determined by the molecular structures, wavelength, and temperature [20–24]. The LC used in the proposed structure is an anisotropic material consisting of rod like molecules which are characterized by ordinary index n_o and extraordinary index n_e. The n_o and n_e of the E7 material were measured previously by J. Li et al. [22] at different visible wavelengths in the temperature range from $15°C$ to $50°C$. The extended Cauchy model was used to fit the measured n_o and n_e which can be described as follows [15, 21–24]

$$n_{e,o} = A_{e,o} + \frac{B_{e,o}}{\lambda^2} + \frac{C_{e,o}}{\lambda^4} \qquad (3)$$

At $25°C$, measured Cauchy coefficients are: $A_e = 1.6933$, $B_e = 0.0078$, $C_e = 0.0028$, $A_o = 1.4994$, $B_o = 0.0070$ and $C_o = 0.0004$.

Figure 1(b) shows the refractive indices of soft glass and LC (both ordinary and extra ordinary) [24]. Glass material which constitutes the core area exhibits higher refractive index than that of the LC in the cladding region. This refractive index contrast structure ensures the guiding of light through the core region. External perturbation on the LC material changes its dielectric properties and ensures tunability of the overall waveguide that will be discussed in later sections.

Even and odd symmetry modes of the structure are supported by both cores of the dual core PCF and the coupling length L_C is

determined by the difference between the wave vector for the even and odd super modes which is formulated as

$$L_c = \frac{\pi}{k_{ze} - k_{zo}} \tag{4}$$

where k_{ze} and k_{zo}, represent the component of wave vectors in the direction of propagation for the even and odd super modes respectively and those can be evaluated by using vector FEM.

2.1. Tuning the Coupler by Heating

Adding an external heat source to the coupler such as thermal heater in the device casing causes change in temperature, this eventually changes the refractive index of the materials. The refractive index of LC has significantly higher temperature sensitivity compared to glass. The temperature effect of the LC refractive indices can be expressed by the average refractive index and birefringence. The four-parameter model for describing the temperature dependence of the LC refractive indices is [21–24]

$$n_e(T) \approx A - BT + \frac{2(\Delta n)_o}{3}\left(1 - \frac{T}{T_c}\right)^{\beta} \tag{5a}$$

$$n_o(T) \approx A - BT - \frac{2(\Delta n)_o}{3}\left(1 - \frac{T}{T_c}\right)^{\beta} \tag{5b}$$

Here T is the temperature in °k and Tc is the clearance temperature for E7 LC it is considered as 340°k [15, 23–24]. The value of the coefficients $[A, B]$ and $[(\Delta n)_\circ, \beta]$ can be found by two-stage fittings. These were evaluated as $A = 1.723$, $B = 0.000524$, $(\Delta n)_\circ = 0.3485$ and $\beta = 0.2542$, at 1550 nm.

As both ordinary and extraordinary refractive indices are temperature sensitive their difference which is the birefringence is also temperature sensitive. Figure 2 shows the wavelength dependent birefringence for temperature of 15–35°C [24]. An increase of birefringence is observed as the temperature decreases. This change of birefringence is somewhat linear for the temperature range from 35°C to 15°C but as suggested by Equation (5) this linear relationship will be change to nonlinear when the temperature get close to the clearance temperature.

The dispersion for the extra ordinary wave is more sensitive than that of the ordinary wave. Figure 3 shows the GVD, β_2 which is the second derivative of the wave vector k_z with respect to angular frequency; ω, and β_3, third order dispersion (TOD) which is the third derivative of the wave vector k_z for the extraordinary wave increases with the increase of temperature. It is also noted that the temperature
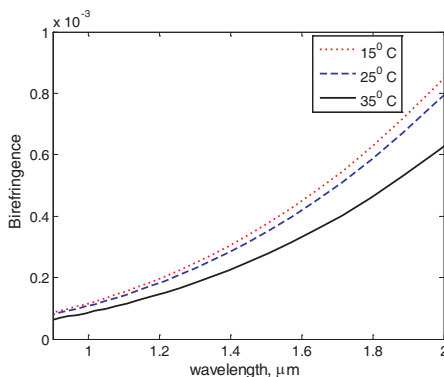
Figure 2. Wavelength dependent birefringence of LC-PCF at different temperature [24].
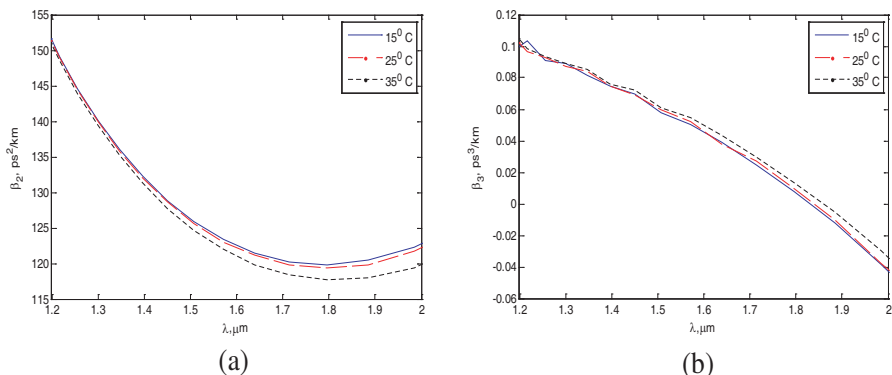

Figure 3. Dispersion of LC-PCF coupler shown in Figure 1 (with $d = 1\,\mu\text{m}$ and $d/\Lambda = 0.4$) at different temperature: (a) GVD. (b) Third order dispersion (TOD).

change effects are stronger in the longer wavelength region. At shorter wavelength, the material dispersion of soft glass dominates the dispersion but at a longer wavelength, waveguide dispersion starts taking over, as does the temperature sensitivity of cladding materials (in this case is LC).

   Coupling Length of the PCF also varies as the temperature increases. The extraordinary wave demonstrates much faster increase of Lc with temperature than that of an ordinary wave. The difference in wave vector for even and odd supper modes is more temperature sensitive for the extraordinary wave than that of the ordinary wave. Figure 4 shows the temperature effects on coupling length [24].
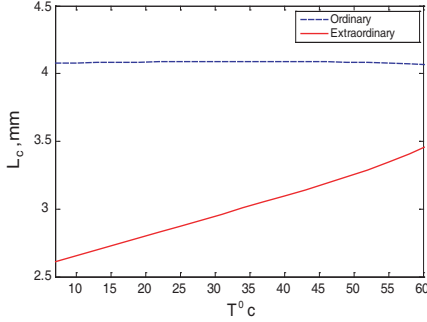
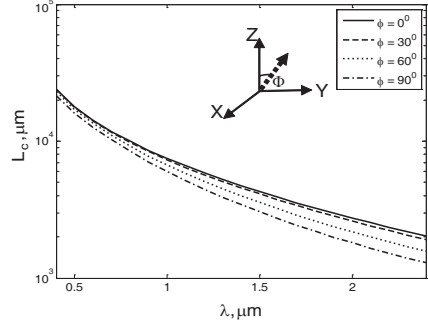**Figure 4.** Coupling length of LC-PCF with temperature variation.

Figure 5. Coupling length variation due to change of director angle of LC in a LC-PCF coupler with $d = 1\,\mu\text{m}$ and $d/\Lambda = 0.4$ at $25°\text{C}$.

2.2. Tuning the Coupler by Applying External Electric Field

Application of an external electric field in the LC-PCF alters the modal characteristics by changing the orientation of the LC molecules' director angle, ϕ. Applying dc voltage in the electrode placed along the ordinary or extraordinary axis provides a preferential orientation for the LC molecules in the corresponding axis. The stronger the applied voltage, the closer the director gets to the corresponding axis (ordinary/extraordinary). The following equation describes the variation of refractive index with the director angle change

$$n = \frac{n_e n_o}{\sqrt{n_e^2 \cos^2 \phi + n_o^2 \sin^2 \phi}} \qquad (6)$$

Orientation of the LC molecule in a particular director angle determines the refractive index. Two boundaries of director angle: $0°$ corresponds to ordinary polarization and $90°$ corresponds to extra ordinary polarization. Figure 5 shows the variation of coupling length due to director angle change. We observe a shorter coupling length as the director angle increases. On the other hand we observe negligible dispersion sensitivity due to the external electric field.

3. SHORT PULSE PROPAGATION

Depending on the excitation wavelength, the PCF couplers are capable of supporting soliton like pulses for the self-focusing nonlinearity of soft glass. Pulse propagation through this coupled structure is described

by [12, 13, 25, 26]

$$\frac{\partial q_1}{\partial z} - \frac{1}{2}(i\Delta\beta q_1 - \Delta\beta_1 \frac{\partial q_1}{\partial \tau}) + i\frac{\beta_2}{2}\frac{\partial^2 q_1}{\partial \tau^2} - \frac{\beta_3}{6}\frac{\partial^3 q_1}{\partial \tau^3}$$
$$-i\gamma(|q_1|^2 + \eta |q_2|^2)q_1 + \frac{\gamma}{\omega}\frac{\partial}{\partial \tau}(q_1 |q_1|^2) + \frac{\pi}{2Lc}q_2 = 0 \qquad (7a)$$

$$\frac{\partial q_2}{\partial z} - \frac{1}{2}(i\Delta\beta q_2 - \Delta\beta_1 \frac{\partial q_2}{\partial \tau}) + i\frac{\beta_2}{2}\frac{\partial^2 q_2}{\partial \tau^2} - \frac{\beta_3}{6}\frac{\partial^3 q_2}{\partial \tau^3}$$
$$-i\gamma(|q_2|^2 + \eta |q_1|^2)q_2 + \frac{\gamma}{\omega}\frac{\partial}{\partial \tau}(q_2 |q_2|^2) + \frac{\pi}{2Lc}q_1 = 0 \qquad (7b)$$

where z and τ are the distance and time respectively; q refers to the envelope of the electromagnetic wave; η is the small ratio of the cross-phase (XPM) to self-phase (SPM) modulation coefficients; $\Delta\beta$ is the phase mismatch evaluated from the difference of k_{ze} for ordinary and extraordinary wave ($\Delta\beta = k_0\Delta n$), $\Delta\beta_1$ is the group velocity mismatch evaluated by taking difference of the first derivative of k_{ze} at two different polarization with respect to angular frequency ω, γ is the nonlinear parameter which can be written as

$$\gamma = \left(\frac{n_2\omega}{cA_{eff}}\right) \qquad (8)$$

where c is the velocity of light, n_2 is the nonlinear index coefficient. Numerically the effective nonlinear modal area, A_{eff}, can be evaluated by using the following expression involving the modal electric field $E(x, y)$ evaluated from the finite element solution of Eq. (1)

$$A_{eff} = \frac{\left(\iint |E(x,y)|^2 \, dxdy\right)^2}{\iint |E(x,y)|^4 \, dxdy} \qquad (9)$$

For the PCF coupler shown in Figure 1 ($d = 1.0\,\mu m$ and $d/\Lambda = 0.4$), A_{eff} was evaluated as $34\,\mu m^2$ at $1.55\,\mu m$. The third and fourth terms in Eq. (7) correspond to the dispersion, the fifth term corresponds to self and cross phase modulation, the sixth term describes the shock effect and the last term corresponds to the linear coupling [12, 13, 25]. These equations were solved numerically using a split step Fourier (SSF) method for 200 fs pulses. The FEM model provided the wave vector k_z, from which the group velocity dispersion, β_2 the second derivative of the wave vector k_z with respect to angular frequency; ω, was calculated. At 25°C and $1.55\,\mu m$ we evaluated β_2 to be $126\,ps^2/km$. Subsequently third order dispersion β_3, the third derivative of the wave vector k_z was evaluated to be $0.055\,ps^3/km$. In the model we incorporate the change of β_2 and β_3 for variable temperature but the effect is not that significant at $1.55\,\mu m$. It is due to the fact that a noticeable change of dispersion was observed only at longer wavelengths as already seen in Figure 3.
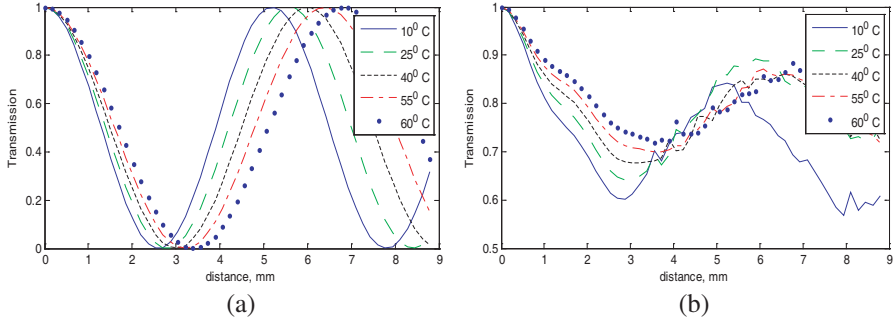
Figure 6. Transmission in bar channel (a) at $0.1 \, \text{GW/cm}^2$, (b) at $2.4 \, \text{GW/cm}^2$ for 200 fs pulse at 1.55 μm with different temperature.

3.1. Tuning the Pulse Switching in LC-PCF Coupler

Pulse intensity determines switching in this device. At low peak intensity of the pulse, the dual core PCF behaves like a linear coupler. The two cores completely exchange power after traveling a distance of L_c. As the intensity increases, an increased fraction of the input power remains in the same waveguide where the pulse was originally launched (bar channel). There is no exchange of energy to the other wave guide (cross channel). Figure 6 shows this clearly. It is worthwhile to mention that the individual polarization modes coupled within each core may change the pulse shape as the frequency component of the pulse varies with state of polarization. However the over all pulse energy at each core which is the sum of all the frequency components remains same and that is the principle cause of switching pulses between the two cores.

As the temperature increases transmission curves for low input power in Figure 6(a) show an increase in L_c. At higher input power Figure 6(b) demonstrate a vertical shifting of transmission curve with the change of temperature. Since the dispersion sensitivity with temperature is negligible at this launching wavelength (1.55 μm), it is the change of L_c with temperature that contributes the most to the tuning of transmission curves. It is worth noting that only the extraordinary wave shows this type of tunability with temperature. Similar tunability in the transmission curve is observed at Figure 7 due to the change of director angle. The 90° shift of director angle which is the extraordinary wave shows the maximum variation in the transmission curve. The L_c is the shortest at that director angle. So the tendency of exchanging energy between core is more in this case.

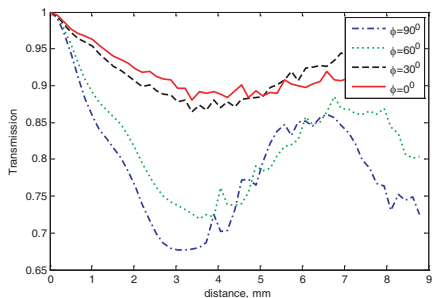The transmission curves for an extraordinary wave with respect

Figure 7. Transmission at $2.4\,\mathrm{GW/cm^2}$ in bar channel with variable director angle for a 200 fs pulse at $1.55\,\mu\mathrm{m}$.
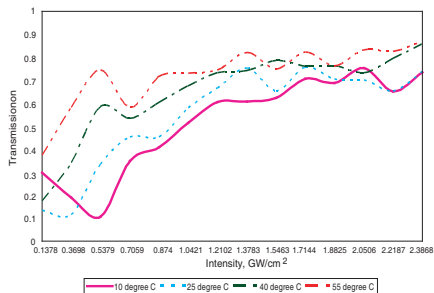
Figure 8. Switching curves of a 9 mm coupler for an extraordinary wave with 200 fs pulse in cross channel at different temperature.

to the intensity at different temperatures are shown in Figure 8. From the figure we see that the switching occurs later at colder temperature. As the temperature increases an earlier switching is observed.

4. CONCLUSION

We have presented the nonlinear switching characteristics of a coupler implemented in a LC-PCF. Our study shows that both the coupling and dispersion properties of PCF can be altered by changing the temperature and external electric field. Material characteristics of E7 type liquid crystal and its sensitivity to heat and electric field is the dominant factor for the tunability of the coupler. The nonlinear properties of the fiber were used to demonstrate all optical switching of short duration pulses.

REFERENCES

1. Bjarkiev, A., J. Broeng, and A. S. Bjarkiev, *Photonic Crystal Fibers*, Kluwer Accedemic Publishers, 2003.

2. Knight, J. C., "Photonic crystal fibres," *Nature*, Vol. 424, 847–851, 2003.

3. Knight, J. C., T. A. Birks, P. S. J. Russell, and D. M. Atkin, "All-silica single-mode optical fiber with photonic crystal cladding," *Optics Lett.*, Vol. 21, No. 19, 1547, 1996.

4. Gander, M. J., R. McBride, J. Jones, D. Mogilevtsev, T. A. Birks, J. C. Knight, and P. S. J. Russell, "Experimental measurement of

group velocity dispersion in photonic crystal fibre," *Electronics Letters*, Vol. 35, 63–64, 1999.

5. Leong, J., P. Petropoulos, J. Price, H. Ebendorff-Heidepriem, S. Asimakis, R. Moore, K. Frampton, V. Finazzi, X. Feng, T. Monro, and D. Richardson, "High-nonlinearity dispersion-shifted lead-silicate holey fibers for efficient 1-μm pumped supercontinuum generation," *Journal of Lightwave Technology*, Vol. 24, No. 11, 183–190, 2006.

6. Cucinotta, A., F. Poli, S. Selleri, L. Vincetti, and M. Zoboli, "Amplification properties of Er3+-Doped photonic crystal fibers," *Journal of Lightwave Technology*, Vol. 21, No. 3, 782–790, 2003.

7. Weirich, J., J. Lægsgaard, L. Scolari1, L. Wei, T. T. Alkeskjold, and A. Bjarklev, "Biased liquid crystal infiltrated photonic bandgap fiber," *Optics Express*, Vol. 17, No. 6, 4442–4453, 2009.

8. Saito, K., N. J. Florous, S. K. Varshney, and M. Koshiba, "Tunable photonic crystal fiber couplers with a thermo-responsive liquid crystal resonator," *Journal of Lightwave Technology*, Vol. 26, No. 6, 663–669, 2008.

9. Hsiao, V. and C.-Y. Ko, "Light-controllable photoresponsive liquid-crystal photonic crystal fiber," *Optics Express*, Vol. 16, No. 17, 12670–12676, 2008.

10. Larsen, T. T., A. Bjarklev, D. S. Hermann, and J. Broeng, "Optical devices based on liquid crystal photonic bandgap fibres," *Optics Express*, Vol. 11, No. 20, 2589–2596, 2003.

11. Saitoh, K., Y. Sato, and M. Koshiba, "Coupling characteristics of dual-core photonic crystal fiber couplers," *Optics Express*, Vol. 11, 3188–3195, 2003.

12. Khan, K. R. and T. X. Wu, "Short pulse propagation in wavelength selective index guided photonics crystal fiber coupler," *IEEE Journal of Selected Topics in Quantum Electronics*, Vol. 14, No. 3, 752–757, 2008.

13. Khan, K. R., T. X. Wu, D. N. Christodoulides, and G. I. Stegeman, "Soliton switching and multifrequency generation in nonlinear photonic crystal fiber," *Optics Express*, Vol. 16, No. 13, 9417–9428, 2008.

14. Gallagher, D. F. G. and T. P. Felici, "Eigenmode expansion methods for simulation of optical propagation in photonics — Pros and Cons," *Proc. SPIE*, Vol. 4987, 69–82, 2003.

15. Hameed, M., S. A Obayya, K. Al-Begain, M. Abo El Maaty, and A. Nasr, "Modal properties of a novel index guiding nematic liquid crystal photonic crystal fiber," *Journal of Light Wave Technology*,

Vol. 27, No. 21, 4754–4762, 2009.

16. Hameed, M. F., S. A. Obayya, K. Al-Begain, A. M. Nasr, and M. I. Abo El Maaty, "Coupling characteristics of a glass nematic liquid crystal photonic crystal fibre coupler," *IET Optoelectronics*, Vol. 3, No. 6, 264–273, Dec. 2009.

17. Hameed, M. F., S. A. Obayya, and R. J. Wiltshire, "Multiplexer-demultiplexer based on nematic liquid crystal photonic crystal fiber coupler," *J. Opt. Quantum Electron.*, Vol. 41, No. 4, 315–326, Mar. 2009.

18. Hameed, M. F. and S. A. Obayya, "Polarization splitter based on soft glass nematic liquid crystal photonic crystal fiber," *IEEE Photonics Journal*, Vol. 1, No. 6, 265–276, Dec. 2009.

19. Jin, J., *The Finite Element Method in Electromagnetics*, Wiley & Sons, 2002.

20. Manufacturer data sheet of SF6 soft glass, Schott North America, Inc.

21. Leong, J., "Fabrication and applications of lead-silicate glass holey fiber for 1-1.5microns: Nonlinearity and dispersion trade offs," Ph.D. Thesis, University of Southampton, Faculty of Engineering, Science and mathematics optoelectronics research centre, 2007.

22. Li, J. and S. T. Wu, "Extended Cauchy equations for the refractive indices of liquid crystals," *J. Appl. Phys.*, Vol. 95, 896, 2004.

23. Li, J., S. Gauza, and S. T. Wu, "Temperature effect on liquid crystal refractive indices," *J. Appl. Phys.*, Vol. 96, No. 19, 2004.

24. Khan, K. and T. Hall, "Tunable liquid crystal filled photonic crystal fiber coupler," *Proceeding of SPIE Photonics Europe*, 2010.

25. Agrawal, G. P., *Nonlinear Fiber Optics*, 3rd edition, Academic Press, 2001.

26. Coen, S., A. H. L. Chau, R. Leohardt, J. D. Harvey, J. C. Knight, W. J. Wadsworth, and P. S. J. Russell, "Supercontinuum generation by stimulated Raman scattering and parametric four-wave mixing in phototonic crystal fibers," *J. Opt. Soc. Am. B*, Vol. 19, 753–764, 2002.